

# Application of Envelope-Following Techniques to the Shooting Method

DANIELE LINARO<sup>1</sup>, DAVIDE DEL GIUDICE<sup>1</sup> (Graduate Student Member, IEEE),  
ANGELO BRAMBILLA<sup>1</sup> (Member, IEEE), AND FEDERICO BIZZARRI<sup>1,2</sup> (Senior Member, IEEE)

<sup>1</sup>DEIB, Politecnico di Milano, 20133 Milan, Italy

<sup>2</sup>Advanced Research Center on Electronic Systems for Information and Communication Technologies E. De Castro, University of Bologna, 41026 Bologna, Italy

CORRESPONDING AUTHOR: F. BIZZARRI (e-mail: federico.bizzarri@polimi.it)

**ABSTRACT** We consider circuits driven by two or more signals with very different periods and propose a method to determine their steady state solution in the time domain. We present a new version of the shooting method based on the envelope following technique. We show how to use the envelope following method as the new engine to efficiently determine the trajectory of the circuit starting from the new guess of the initial conditions. It substitutes the less efficient time domain analysis used in the conventional implementation of the shooting method. We show that it is well suited to circuits where the ratio between the periods of the slow and fast behaviour is particularly high and characterised by strong non-linearities. The numerical properties at the basis of the proposed method are presented. Its features are shown by simulating different types of slow-fast circuits.

**INDEX TERMS** Slow-fast circuit, shooting method, envelope following method, time domain circuit simulation, multi-tone driven circuit, circuit simulation.

## I. INTRODUCTION

THE PROBLEM of efficiently determining the steady-state solution of circuits driven by two or more signals with very different periods is still challenging and not fully solved. One of the main problems is numerical efficiency. Among the numerous modern circuits that fall into this category are for example integer phase locked loops (PLLs) used in RF applications, characterised by a very large ratio between the frequency of the reference signal and that of the voltage controlled oscillator (VCO) (typically a few MHz for the former vs. several GHz for the latter). In a type-II PLL, the frequency divider and part of the phase-frequency detector are in general modeled as digital circuits. The ratio between the frequency of the reference signal to which the PLL locks and that of the VCO output can be greater than 100 [1]. This means that one has to accurately simulate 100 working periods of the VCO for each period of the reference signal. Furthermore, this drawback cannot be overcome by representing the solution in the frequency domain through a Fourier series, as the digital nature of the circuit badly adapts to such a representation.

Another example of circuits where this problem naturally arises are switched mode power supplies (SMPS), found, for

instance, in most battery chargers: these, too, are characterized by a very large ratio between the switching frequency (up to a few MHz) and that of a control or disturbance signal (for instance, around 100 Hz for input ripple). In SMPS, the energy is drawn in packets from a source, stored in an inductor, and later released packet-wise to the load. SMPS have switching transistors, and the input to the controller can be driven by a relatively slow signal with respect to the period of the switching signal (for example 100 Hz vs. 100 kHz). In the time domain, we must therefore simulate 1000 periods of the switching signal for each period of the driving signal.

Several methods were developed to find the steady-state solution of these circuits both in the frequency domain and in the time domain or in a mixed frequency-time domain (for a review, see [2]). We briefly describe here the main methods.

### A. PREVIOUS WORKS: HARMONIC BALANCE, SHOOTING AND MULTIVARIATE FORMULATION

Frequency-domain numerical algorithms, such as the harmonic balance (HB), represent the periodic solution through a Fourier series. The differential algebraic equations (DAEs)

modeling the dynamic circuit are transformed into algebraic equations in the frequency domain. HB determines the coefficients of the Fourier series representing the periodic solution. The total number of considered harmonics affects the reliability of the solution, mainly on the convergence of the method by limiting aliasing. As a simple rule, a higher circuit non-linearity suggests using a larger number of harmonics. HB suffers from the problem of harmonic proliferation, which depends on the degree of non-linearity of the circuit and on the number of driving signals. Let us consider a circuit driven by two signals characterized by two well-separated fundamental frequencies, for instance 1 kHz and 1 GHz. If we employ  $H_1 = 64$  and  $H_2 = 32$  harmonics to represent these two signals, their beats lead to a total of  $64 \times 32 = 2048$  harmonics (“square” mapping) [3]. Each electrical quantity of the circuit is then represented by a vector of 2048 entries, i.e., the coefficients of the Fourier series. If the circuit model has  $N$  unknowns, the HB problem is composed of  $2048 \times N$  equations. This figure can easily grow up to some millions even in the case of small- or medium-sized circuits. The use of specialized solvers, based for example on GMRES, only partially mitigates the numerical burden [4]. Additionally, even in relatively small circuits characterized by strong non-linearities,  $N_1$  and  $N_2$  may become very high: this is typical, for example, for SMPS and PLLS.

The counterpart of HB in the time domain is the shooting (SH) method [3], [5], [6]. This algorithm finds values of the state variables of the system that lie on the stable limit-cycle constituting the solution of an initial-value problem. This problem is cast as a nonlinear boundary-value problem, which is solved by means of the Newton iterative method. The SH method has the advantage of handling well the non-linearities of the system. The main disadvantage consists in requiring a time domain simulation of the circuit lasting a full working period, since the value of the solution at the end of one period must be computed by starting from the value of the initial conditions at the beginning of the period. This may take a large amount of CPU time. Additionally, the Newton method requires the computation of the sensitivity matrix, which captures how the solution at the last time point of the period depends on the initial conditions. This implies that at each time step of the time domain analysis, a matrix by matrix product (of size comparable to the number of state variables) has to be performed, thus significantly slowing down the computation [7]. Computing the steady state solution of these slow-fast circuits is challenging also for what concerns *accuracy* and *numerical stability* due to accumulations of numerical errors. For this reason, and also to parallelize the computation of the trajectory at each iteration of the SH method, multiple-shooting techniques have been proposed [8].

Finally, in multi-variate formulation (MVF) the slow-fast behaviour is represented by exploiting two distinct and discrete time axes that can be represented in the orthogonal Cartesian plane [9], [10]. The values of the two periods define a rectangle in this plane in which the solution lays.

The DAES modeling the circuit are transformed in a partial derivative problem on a suitable time point grid in this rectangle. The computational burden may be very high since a solution of the partial differential problem must be found on each point of the grid. Furthermore an optimal time grid is unknown a priori but only after the computation of the solution, which is obviously the objective of this family of algorithms [11]. We refer the reader interested in modifications to these methods that mitigate their drawbacks to [2] and references therein.

## B. CONTRIBUTIONS

The methods described previously display advantages and drawbacks depending on the circuit characteristics and usage context. The common drawback that affects them is the lack of robust numerical efficiency in a wide range of circuit applications. Our contribution is aimed in this direction, i.e., towards improving at least one aspect of numerical efficiency. Since we also aim at dealing with mixed analog/digital circuits displaying strong non-linearities, we chose to improve SH. In this paper we thus present a new algorithm to determine the steady-state solution in the time domain of strongly non-linear circuits driven by more than one tone. The core and novelty of our algorithm relies on the usage of the envelope following method (EFM) [12]–[18] to accelerate the computation of the solution over one full period of the system under analysis. As stated earlier, this is the most CPU-time-consuming component of the conventional SH procedure, since it is performed at each iteration of the Newton method to improve the estimation of the initial conditions that lead to a steady-state solution. EFM improves the efficiency in the computation of the trajectory and of the sensitivity matrix, thereby enhancing the overall efficiency of the SH algorithm. EFM has been previously used in similar contexts such as to speed-up of the computation of the solution of MVF [2], [19], [20].

EFM was initially developed and is widely used to accelerate the time domain analysis with a marginal and acceptable sacrifice of accuracy [12], [13], [16], [18], [21]. Compared to conventional time-domain simulation, the envelope-following approach leads to a great increase in efficiency since only a limited number of short (fast) periods of the system need to be computed for each long (slow) period. EFM can not be used “as is” as a numerical booster in the SH method. As a consequence, we enhanced and improved EFM to fit the requirements of the SH method, notably by acting on the computation of the sensitivity matrix, which is the main numerical bottleneck of the conventional SH method when dealing with large circuits.

## II. BASICS OF THE ENVELOPE-FOLLOWING TECHNIQUE

First introduced in [22], the envelope-following technique is an algorithm that can be employed to efficiently compute the solution of a set of highly oscillatory ordinary differential equations (ODEs), characterized by the presence of a fast oscillation and of a slowly-changing envelope.

Basically, the method consists in computing the conventional solution to the set of ODEs over a limited number of short periods (i.e., those characterized by a high oscillation frequency), and then use this information to “sample” the slowly-changing envelope using a large time step, typically at time instants that are integer multiples of the period of the fast oscillation, even though this is not a strict requirement of the technique [22]. The main advantage of this method, compared to the computation of the full solution of the system of ODEs by a conventional solver, is a substantial reduction in the time required to compute the solution. This in turn comes at the cost of ignoring the detailed solution over the full integration interval. As anticipated in the introduction, in many practical applications such as the simulation of PLLs and SMPS, the lack of details on the full solution does not pose any problem. This method has therefore been successfully employed for such applications [12], [18], [23], [24].

More formally, the EFM can be used to find the solution of a system of ODEs of the form

$$\dot{x} = f(t, x), \quad (1)$$

where  $f$  is the vector field,  $x \in \mathbb{R}^n$  is the *state* of the system and  $x(t_0) = x_0$  is the initial condition. The only assumption of the method is that  $x(t)$  be periodic or quasi-periodic over the integration interval. In other words, as we will see more in detail in the following,  $x(t)$  must intersect a properly defined Poincaré section with (potentially varying) period  $T$ . If this is the case, we can define the *envelope vector field* as

$$g(T, x(t), x(t+T)) = \frac{1}{T}[x(t+T) - x(t)], \quad (2)$$

where we have integrated system (1) from  $t$  to  $t+T$  with conventional methods.

Our implementation of the EFM closely resembles that described in [23]. Briefly, given the envelope vector field in Eq. (2), we can predict the next value of the envelope solution by using an explicit Euler integration scheme [25]:

$$x(mT) = x(nT) + Hg(T, x(nT), x((n+1)T)), \quad (3)$$

where  $H = (m-n)T$  with  $m-n \geq 1$  is the *envelope time step*. The predicted  $x(mT)$  envelope solution obtained with Eq. (3) can be corrected using an implicit method, such as backward Euler [25]:

$$x(mT) = x(nT) + Hg(T, x(mT), x((m+1)T)), \quad (4)$$

or the trapezoidal rule:

$$x(mT) = x(nT) + \frac{H}{2}(g(T, x(nT), x((n+1)T)) + g(T, x(mT), x((m+1)T))). \quad (5)$$

Even though for simplicity we referred to the ODE formulation, the proposed method was developed and implemented considering semi-explicit index-1 DAEs. Some basic aspects concerning the tight relationship between the latter and ODEs are reported in Appendix.

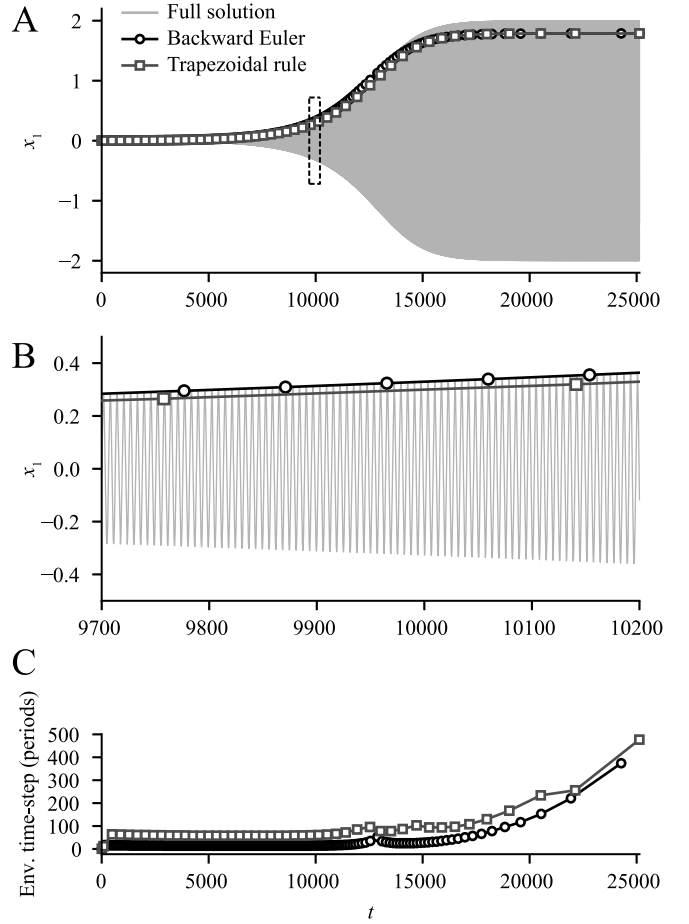


**FIGURE 1.** An application example of the EFM to the solution of the autonomous Van der Pol oscillator. (A) Envelope solutions obtained by means of the backward-Euler scheme (black trace with circular markers) and of the trapezoidal rule (grey trace with square markers) superimposed to the full solution (light grey trace). (B) Enlargement of the area in the boxed region in A. (C) Envelope time-step in units of period of the original system.

An example of the application of the EFM is shown in Fig. 1; the system models the well-known autonomous Van der Pol oscillator [26], [27], described by the following set of ODEs

$$\begin{cases} \dot{x}_1 = x_2 \\ \dot{x}_2 = \epsilon(1 - x_1^2)x_2 - x_1, \end{cases} \quad (6)$$

where we chose  $\epsilon = 10^{-3}$ . Small values of  $\epsilon$  cause the solution of the system to very slowly approach the (stable) steady-state limit cycle, especially when starting close to the (unstable) equilibrium point located in the origin of the system of coordinates. From a circuitual point of view, this corresponds to implementing a high-Q quality factor resonator. This implies that a large number of fast oscillations of the system must be computed before the solution reaches its steady-state orbit<sup>1</sup> by starting from an initial condition very close to the unstable equilibrium point.

1. Orbits of a continuous-time system with a continuous evolution operator  $\varphi^t$  are curves in the state space parametrized by time  $t$  and oriented by its direction of increase. A cycle is a periodic orbit, namely a non-equilibrium orbit  $L_0$ , such that each point  $x_0 \in L_0$  satisfies  $\varphi^{t+T_0}x_0 = \varphi^t x_0$  with some  $T_0 > 0$ . The minimal  $T_0$  with this property is called the period of the cycle  $L_0$ . See [28] for more rigorous definitions.

We employed both backward-Euler and the trapezoidal methods in the envelope solution and compared the results to a conventional time-domain integration obtained by means of the `solve_ivp` routine available in the SciPy Python module [29]. We chose the almost null initial condition  $x = [0.002, 0.001]$ , which leads to a long, slowly evolving transient, appropriate to illustrate the features of the EFM. As it can be seen in Fig. 1A, individual periods in the conventional solution (light grey trace) cannot be discerned at this scale, while the individual points of the envelope solutions (black line and circles for the backward Euler method and grey line and squares for the trapezoidal rule) are clearly visible. Figure 1B shows an enlargement of the boxed region in panel A, where individual oscillations of the conventional time domain solution are visible. We can appreciate how the trapezoidal rule, being more accurate (higher order [12], [23]), allows taking longer steps on the envelope waveform than backward Euler, for the same values of absolute and relative tolerance. For this reason, in the remainder of this article, we will employ the trapezoidal rule implementation of the EFM. Finally, Fig. 1C shows the time-step of both EFMs, which is a multiple of the fast period of the Van der Pol oscillator, in this case equal to  $2\pi$ . Notice how the time-step used to compute the envelope progressively increases as the solution of the Van der Pol system reaches the steady-state. The figure clearly shows that the numerical efficiency in computing the solution increases by several orders of magnitude, which is indeed the main strength in the adoption of the EFM. A larger time step in integrating the envelope means a larger number of periods of the fast waveform that are skipped, thus increasing numerical efficiency.

It is worth noting that the application of the EFM by itself is advantageous also in the absence of two different time-scales, as is the case for the example shown in Fig. 1, which displays a slowly-evolving transient leading to the steady-state oscillatory solution. The steady state solution of the Van der Pol oscillator can be found in a very efficient way by the conventional SH method. In the following, we will focus on systems exhibiting a periodic solution whose period is the least common multiple (LCM) of at least two very different values, as in the case of the Van der Pol oscillator with a very low frequency forcing signal. We show that the EFM is particularly suited to enhance the performance of the SH method applied to this category of systems.

### A. THE SHOOTING METHOD

Here, we employ the shooting method as described in [5], [30]. Briefly, this technique can be used to efficiently locate stable periodic solutions of a system of ODEs, such as the one described in (1), by solving an appropriate boundary value problem (BVP) imposing the condition

$$x(t_0 + \widehat{T}) = x(t_0), \quad (7)$$

where  $t_0$  is an arbitrary initial time and  $\widehat{T}$  is the period of the system. In order to solve this BVP, one can extend the

original system (1) with the so-called *variational system* [31], thus obtaining the following system of equations

$$\begin{cases} \dot{x}(t) = f(t, x) \\ \dot{\Phi}(t, t_0) = J(t, x)\Phi(t, t_0) \\ x(t_0) = x_0 \\ \Phi(t_0, t_0) = \mathbf{1}, \end{cases} \quad (8)$$

where  $J(t, x) \in \mathbb{R}^{n \times n}$  is the time-varying Jacobian matrix of  $f$ ,  $\Phi(t, t_0) \in \mathbb{R}^{n \times n}$  is the *fundamental matrix* associated with system (1), and  $\mathbf{1}$  is the  $(n \times n)$  identity matrix. To find a value of  $x_0$  satisfying Eq. (7), one typically employs an iterative scheme such as the Newton method: for an in-depth discussion of the SH method, see [32], [33]. For our purposes, it is sufficient to recall that the  $x_0^{k+1}$  guess of the initial condition  $x_0$  at the  $(k+1)$ -th iteration step is given by

$$\begin{aligned} r &= x^k(t_0 + \widehat{T}) - x_0^k \\ M &= \Phi(t_0 + \widehat{T}, t_0) - \mathbf{1} \\ x_0^{k+1} &= x_0^k - M^{-1}r. \end{aligned} \quad (9)$$

This procedure is repeated until the difference between  $x_0^{k+1}$  and  $x_0^k$  is within an accepted tolerance. The following important aspects should be taken into consideration:

(i) at each  $k$ -th iteration, a time domain analysis must be performed lasting a whole period  $\widehat{T}$  of the circuit. When the system under analysis is a slow-fast dynamical system admitting a periodic steady-state behavior, we can assume that  $T_s$  and  $T_f$  stand for the steady-state periods of the slow and fast dynamics of the overall system, respectively. In this case,  $\widehat{T} = pT_s = qT_f$ , with  $T_f \ll T_s$  and  $p \ll q$ . Thus we assume that the steady state behavior of the slow-fast system is synchronized in frequency with the LCM between  $T_s$  and  $T_f$ . Since  $\widehat{T} = pT_s$  is typically several orders of magnitude larger than the period of the fast oscillation, the integration time step must be substantially smaller than  $\widehat{T}$  to accurately grasp all the details of the underlying fast dynamics.

(ii) We must compute the  $\Phi(t_0 + \widehat{T}, t_0)$  state transition matrix and this requires a matrix multiplication of size  $n \times n$  at each time step of the time domain analysis. As anticipated in the introduction, these two aspects are the main numerical bottlenecks of the SH method.

### III. THE EFM BASED SHOOTING METHOD

In this section we outline the implementation of our algorithm for the computation of the steady-state solution of slow-fast systems by means of a suitable joint approach between the SH method and EFM.

It rests on the idea that the computation of an oscillatory steady-state solution of the slow-fast dynamical system (1) by means of the SH method can be sped up by resorting to the EFM. This is done by applying the EFM to the variational problem (8) that must be solved at each iteration of the SH method. The main idea is to solve (1) by using Eq. (2) while trying to reduce as much as possible the effort required to compute  $\Phi(t, t_0)$ : as we will see shortly, this can be done by resorting to the very properties of  $\Phi(t, t_0)$  [32].

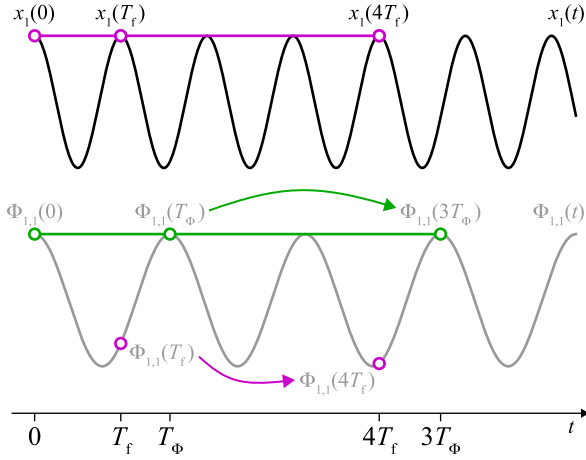


**FIGURE 2.** Graphical representation of the EFM applied to a system with oscillating variational components.  $x_1(t)$  is the first component of the system, whereas  $\Phi_{1,1}(t)$  is the first component of the corresponding variational problem. The solid traces represent the solution of the integration of the full system, while the dots are the points at which the envelope of the full system is computed.

To improve readability, the method we are proposing is explained through examples, trying to reduce mathematical formalism as much as possible. Furthermore, we assume  $\hat{T} = T_s$ , i.e.,  $p = 1$ .

The variational part of the extended system (8) does not necessarily exhibit oscillatory dynamics, since not all elements of  $\Phi(t, t_0)$  oscillate. Furthermore, if  $\Phi(t, t_0)$  is oscillatory, the oscillation period, say  $T_\Phi$ , is in general different from  $T_f$  (or from one of its integer multiples) and typically unknown.

### A. THE EFM APPLIED TO THE EXTENDED SYSTEM

Since in general  $T_\Phi \neq T_f$ , if one chose to compute the envelope of the extended system at time instants that are (integer) multiples of  $T_f$ , the corresponding time points at which the solution of the variational system will be computed would not constitute its envelope, and the same would hold if  $T_\Phi$  were chosen. To clarify this point, let us consider the waveforms in Fig. 2 in which, without lack of generality,  $T_f < T_\Phi$ . The black and grey solid traces represent, respectively, the  $x_1(t)$  variable of the system and the  $\Phi_{1,1}(t, t_0 = 0)$  variable of the variational system.  $\Phi_{1,1}(t, t_0 = 0)$  is the element in the first row and first column of the matrix  $\Phi$ . Starting from the initial condition at time  $t_0 = 0$ , the algorithm first integrates the extended system from 0 to  $T_f$ , finding both points  $x_1(T_f)$  of the solution of the system and  $\Phi_{1,1}(T_f, 0)$  of the variational system. The points  $x_1(0)$  and  $x_1(T_f)$  are used to estimate the envelope vector field in Eq. (2) and to project the solution until time  $\kappa T_f$ , where the point  $x_1(\kappa T_f)$  is located (in the example shown in Fig. 2,  $\kappa = 4$ ). As we can see,  $x_1(\kappa T_f)$  is located on the envelope waveform: however, one cannot use points  $\Phi_{1,1}(0, 0)$  and  $\Phi_{1,1}(T_f, 0)$  to estimate  $\Phi_{1,1}(\kappa T_f, 0)$ , i.e., the value of the variational system at time  $\kappa T_f$ , because point  $\Phi_{1,1}(\kappa T_f, 0)$  does not belong to the envelope of the variational system. Note that these points belong to the solution of the variational system but are located at

time instants that do not allow us to extrapolate the envelope waveform.

To overcome this issue one could use the EFM to integrate (8) until  $t = T_\Phi$  and then compute (i) the vector field of the envelope of (1) by using the points  $x_1(0)$  and  $x_1(T_f)$  and (ii) the vector field of the envelope of  $\Phi(t, t_0)$  by using the points  $\Phi_{1,1}(0, 0)$  and  $\Phi_{1,1}(T_\Phi, 0)$ . If the next point of the envelope of (1) is estimated to be  $x_1(\kappa T_f)$ , which is located at  $t = \kappa T_f$ , the algorithm computes the number of periods of the variational system such that the very next point of the envelope of the variational system is located at  $\chi T_\Phi$  after the new point of the system, being  $\chi$  the smallest integer number such that  $\chi T_\Phi > \kappa T_f$ . In Fig. 2  $\chi = 3$ , thus the  $\Phi_{1,1}(3T_\Phi, 0)$  point belongs to the envelope of the variational system.

Once a good set of points belonging to the envelope of the variational system have been extrapolated, they can be used to estimate the local truncation error (LTE) of the variational system with the same procedure employed for the LTE of the original system [23]. It is therefore possible to impose a tolerance on the LTE of the envelope of the variational system, which, alongside the tolerance on the LTE of the envelope of the system, governs the step-size used in the calculation of the envelope of the full, extended system. This means that we use a variable step-size integration algorithm in computing the envelope, i.e., the slow dynamics of the circuit: this adapts the step-size according to the time scale of the slow dynamics.

### B. USING THE COMPOSITION PROPERTY OF THE TRANSITION MATRIX

The method presented in the previous section suffers from numerical burden since the envelope vector field is used to compute  $\Phi(\chi T_\Phi, 0)$ . An alternative and efficient approach to compute  $\Phi(\chi T_\Phi, 0)$  is to resort to the *composition property* of the  $\Phi(t, t_0)$  matrix<sup>2</sup> [32]. A guess for  $\Phi(\chi T_\Phi, 0)$  can be obtained as  $\Phi^{\chi-1}(T_\Phi, 0)$ , i.e., raising the  $\Phi(T_\Phi, 0)$  matrix to a power whose coefficient is equal to the time difference between  $T_\Phi$  and  $\chi T_\Phi$  in units of  $T_\Phi$ . This procedure of computing the envelope of the original system and then *dragging* the solution of the variational system to the corresponding time instants is repeated for the whole duration of the envelope integration. This is one of the main results of the paper since dragging increases the numerical efficiency in computing the sensitivity matrix of a highly oscillatory system. Raising of the  $\Phi(T_\Phi, 0)$  matrix is performed through a suitable sequence of matrix multiplications that leads to the final value of  $\Phi(\chi T_\Phi, 0)$ . For example, consider  $\chi = 53$  and the sequence of partial matrix products:

$$\begin{aligned}\Phi^2(T_\Phi, 0) &= \Phi(T_\Phi, 0) \Phi(T_\Phi, 0) \\ \Phi^4(T_\Phi, 0) &= \Phi^2(T_\Phi, 0) \Phi^2(T_\Phi, 0) \\ \Phi^8(T_\Phi, 0) &= \Phi^4(T_\Phi, 0) \Phi^4(T_\Phi, 0) \\ \Phi^{16}(T_\Phi, 0) &= \Phi^8(T_\Phi, 0) \Phi^8(T_\Phi, 0)\end{aligned}$$

2. The composition property of  $\Phi(t, t_0)$  allows one to compute the latter as  $\Phi(t, t_0) = \Phi(t, \hat{t})\Phi(\hat{t}, t_0)$  being  $t_0 \leq \hat{t} \leq t$  [31].

$$\begin{aligned}\Phi^{32}(T_\Phi, 0) &= \Phi^{16}(T_\Phi, 0) \Phi^{16}(T_\Phi, 0) \\ \Phi^{48}(T_\Phi, 0) &= \Phi^{32}(T_\Phi, 0) \Phi^{16}(T_\Phi, 0) \\ \Phi^{52}(T_\Phi, 0) &= \Phi^{48}(T_\Phi, 0) \Phi^4(T_\Phi, 0) \\ \Phi^{53}(T_\Phi, 0) &= \Phi^{52}(T_\Phi, 0) \Phi^1(T_\Phi, 0).\end{aligned}$$

It is clear that instead of performing 53 matrix by matrix products, as the conventional SH does, only 8 matrix by matrix products are performed. We thus obtain the  $\Phi(T_s, t_0)$  matrix, which represents the sensitivity of the solution at the end of the working period of the circuit with respect to the given initial conditions at the beginning of the working period. As stated earlier, the SH method uses  $\Phi(T_s, t_0)$  to compute the correction of the initial condition necessary to close the periodic orbit.

### C. NON-SMOOTH SLOW-FAST DYNAMICAL SYSTEMS

It is well-known that the SH method cannot be directly applied to non-smooth systems. In these dynamical systems, the vector field is either not everywhere differentiable or the flow function is not continuous. Consequently, it is not possible to linearise their dynamics around a reference trajectory, viz. the variational system in (8) is not defined *everywhere* along the latter. To overcome this issue, one can derive the zero-time discontinuity mapping associated with the discontinuity boundary [34]. The Jacobian of this mapping is known as *saltation matrix*. Its properties reveal how the crossing of the discontinuity boundary affects the deviations of perturbed trajectories from a reference trajectory. In this way, it is possible to *correct* the fundamental matrix at the discontinuity boundary and extend (8) to non-smooth systems. So doing, several techniques that are typically adopted to study smooth systems can be profitably extended to non-smooth ones [5], [6], [35]. SH method is among those. Section IV-B deals with an example of a slow-fast non-smooth electronic circuit and shows how SH method combined with EFM can be used to compute its periodic steady-state orbit.

## IV. NUMERICAL RESULTS

### A. VAN DER POL OSCILLATOR

We present the main features of the proposed algorithm by using as a benchmark a version of the forced Van der Pol oscillator [26], [27], described by the following set of ODEs:

$$\begin{cases} \dot{x}_1 = x_2 \\ \dot{x}_2 = \epsilon(1 - x_1^2)x_2 - x_1 + A_1 \sin(2\pi f_s t) + A_2 \sin(2\pi f_f t), \end{cases} \quad (10)$$

where  $A_1$  and  $A_2$  are constant terms that regulate the (relative) strength of the forcing waveforms and  $f_s$  and  $f_f$  are the (slow and fast) forcing frequencies. In order to introduce a slow and a fast oscillation in system (10), we set  $f_s = 4$  Hz and  $f_f = 200$  Hz, leading to an overall period of the oscillations equal to  $T_s = 1/f_s$ . Additionally, as shown in Fig. 3A, this corresponds to having 50 fast oscillations for each slow

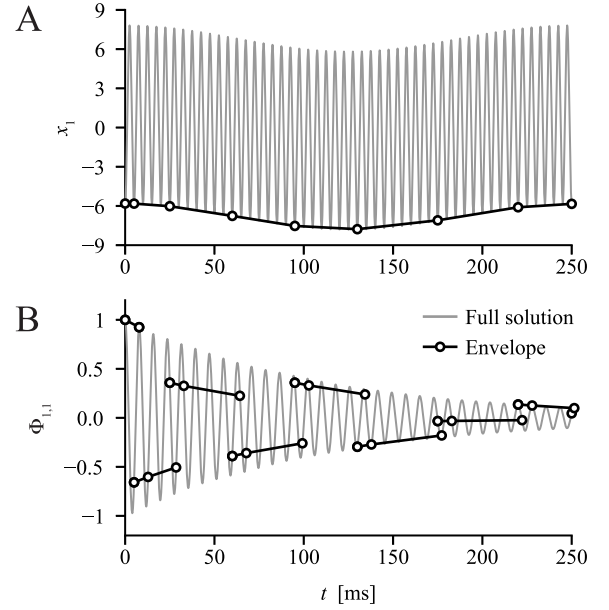


**FIGURE 3.** Comparison between full and envelope solutions of the extended Van der Pol system. The grey traces are the solutions obtained when integrating system (12) with the SciPy function `solve_ivp`, while the black dots represent the envelope of the system. In panel B, the triplets of points are “pieces” of the envelope of the variational system and are used to estimate the envelope LTE on the variational system, which dictates the overall envelope time-step.

one, a condition that is well suited for analyses using the envelope-following technique.

The Jacobian matrix of the Van der Pol oscillator in (10) is

$$J = \begin{bmatrix} 0 & 1 \\ -2\epsilon x_1 x_2 - 1 & \epsilon(1 - x_1^2) \end{bmatrix} \quad (11)$$

and consequently the full, variational system is given by the following set of six ODEs:

$$\begin{cases} \dot{x}_1 = x_2 \\ \dot{x}_2 = \epsilon(1 - x_1^2)x_2 - x_1 + A_1 \sin(2\pi f_s t) + A_2 \sin(2\pi f_f t) \\ \dot{\Phi}_{1,1} = \Phi_{2,1} \\ \dot{\Phi}_{1,2} = \Phi_{2,2} \\ \dot{\Phi}_{2,1} = -[(2\epsilon x_1 x_2 + 1)\Phi_{1,1} + \epsilon(x_1^2 - 1)\Phi_{2,1}] \\ \dot{\Phi}_{2,2} = -[(2\epsilon x_1 x_2 + 1)\Phi_{1,2} + \epsilon(x_1^2 - 1)\Phi_{2,2}]. \end{cases} \quad (12)$$

We integrated system (12) on the interval  $[0, T_s]$  starting from the initial condition  $(-5.8133, 0.1347, 1, 0, 0, 1)$  using both the SciPy [29] function `solve_ivp` and our implementation of the envelope-following algorithm. Figure 3 shows the results for variables  $x_1$  and  $\Phi_{1,1}$ : the grey lines represent the full solution obtained with `solve_ivp`, whereas the black dots are the points at which the envelope is computed. The full and envelope-accelerated solutions are composed of 2904 and 11 time points, respectively, which means that, with respect to SH, the proposed shooting-envelope method in this case computes only 0.4% as many matrix products as the conventional algorithm. Note that, unlike the original implementation presented in [22], which

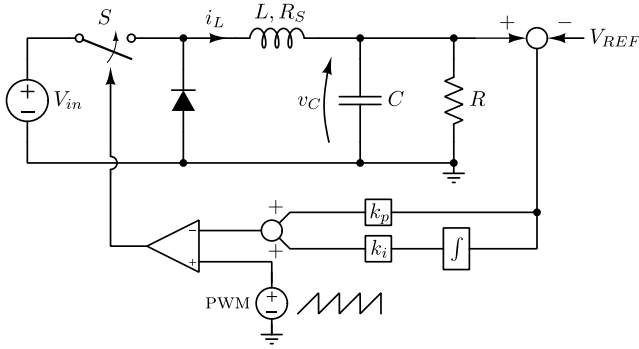


**FIGURE 4.** Schematic of a PWM-controlled DC-DC buck converter. Fixed parameter values are:  $V_{REF} = 10\text{ V}$ ,  $k_p = 0.1$ ,  $k_i = 10$ ,  $R = 6\ \Omega$ ,  $C = 20\ \mu\text{F}$ ,  $L = 1\ \text{mH}$ ,  $R_S = 10\ \text{m}\Omega$ .

allows for integration time-steps that are not integer multiples of the fast oscillation period, in our implementation the envelope points belong to the full solution of system (12). Notably, in this particular example the variational part of system (12) oscillates with a period equal to  $T_\Phi = 2\pi/T_s$ . This is represented in Fig. 3B by the triplets of points on the solution of  $\Phi_{1,1}$ . The first point of each triplet is located at the same time instant as the envelope points shown in the top panel. The second point is at a distance of  $T_\Phi$  from the first one and allows calculating the variational envelope vector field by using Eq. (2), therefore to compute the third point in the triplet. The last point in each triplet is located *after* the next point of the full envelope. As previously discussed, this allows calculating the LTE by using the triplet's points to determine whether the envelope step-size should be reduced or increased for better numerical efficiency.

Finally, it is important to note that the last point of the envelope corresponds to the final point of the periodic orbit. This is crucial in order to estimate the correction required by the SH method to compute the steady-state solution of system (10). As a measure of the proximity at  $t = T_s$  between the solutions by conventional integration and by our method, we computed the eigenvalues of the matrix  $\Phi$ , obtaining  $[0.04921 + j0.09062]$  when integrating (12) with `solve_ivp` and  $[0.04987 + j0.09136]$  when using our method, indicating a good agreement between results.

## B. BUCK CONVERTER

As an example of a switching system, in this section we consider the PWM-controlled buck converter with proportional-integral (PI) controller [36] shown in Fig. 4 and described by the following set of equations:

$$\dot{x} = \begin{cases} Ax + B_1 & \text{if } \sigma(x, t) > 0 \\ Ax + B_2 & \text{if } \sigma(x, t) < 0, \end{cases} \quad (13)$$

where  $x = [v_C, i_L, \int (v_C - V_{REF})]^T$  is the state vector and the matrix  $A$  and vectors  $B_1$  and  $B_2$  are given by

$$A = \begin{bmatrix} -\frac{1}{RC} & \frac{1}{C} & 0 \\ -\frac{1}{L} & -\frac{R_S}{L} & 0 \\ 1 & 0 & 0 \end{bmatrix}, \quad B_1 = \begin{bmatrix} 0 \\ \frac{V_{in}(t)}{L} \\ -V_{REF} \end{bmatrix}, \quad B_2 = \begin{bmatrix} 0 \\ 0 \\ -V_{REF} \end{bmatrix},$$

where  $R$  is the output load resistance,  $L$  is the inductance with an equivalent series resistance  $R_S$ ,  $C$  is the capacitance and  $V_{in}(t)$  is the input voltage. Full details on this example can be found in [36]. The comparator has as inputs the PWM saw-tooth waveform and the output of the PI block. Each time the PWM ramp goes above the PI output signal the  $S$  switch closes and vice versa. In a formal way, the comparator introduces the  $\Sigma$  manifold,<sup>3</sup> given by

$$\sigma(x, t) = v_{\text{PWM}}(t) - k_p(v_C(t) - V_{REF}) + k_i \int_0^t (v_C(\tau) - V_{REF}) d\tau = 0, \quad (14)$$

where  $v_{\text{PWM}}$  is the PWM reference voltage (purple trace in Fig. 5C). The buck converter we consider here is characterized by the presence of two different time scales: the first one has the same period of the PWM, which we shall call  $T_f$ , while the second one is due to the slow (compared to  $T_f$ ) oscillation of the input voltage that models ripple due to the rectifier, i.e.,  $V_{in}(t) = V_{in,0} + \Delta V_{in} \sin(2\pi f_s t)$ , with  $V_{in,0} = 20\text{ V}$ ,  $\Delta V_{in} = 2\text{ V}$  and  $f_s = 100\text{ Hz}$ . The ratio between  $T_s = 1/f_s$  and  $T_f$  sets the number of “fast” oscillations contained in each period of the modulating signal.

Figure 5 shows an example of the dynamics of the system, which highlights the presence of a fast oscillation due to the PWM (here,  $T_f = 50\ \mu\text{s}$ ) and a slow oscillation due to the sinusoidal modulation of the input voltage.

Given its slow-fast nature, the buck converter is well suited to the application of the EFM to speed-up the shooting analysis. In particular, changing the ratio between slow and fast dynamics of the system by varying the frequency of the PWM should directly affect the speed-up due to the application of the EFM. To test this, we varied  $T_f$  in the range  $[5, 100]\ \mu\text{s}$ , corresponding to a number of fast periods in each slow oscillation ranging from 100 to 2000. For each value of  $T_f$ , we performed a shooting analysis, with and without envelope-following-based acceleration and compared both the accuracy of the results and the computation times. We point out that the variational part of this system does not have periodic oscillatory behavior, and therefore our algorithm does not use the information about the variational LTE to compute the step-size used in the computation of the envelope of the system.

As shown in Fig. 6A, we found that the speed-up due to the application of the EFM grows linearly with the ratio between slow and fast periods, with negligible losses in terms of accuracy of the solution, as shown in Fig. 6B-C. In this figure we compare the initial conditions of the final shooting iteration (i.e., the stable limit cycle of the system, computed over a full period  $T_s = 1/f_s$ ) obtained with conventional ( $x$ -axis) and envelope-following-based ( $y$ -axis) algorithms.

As a final test of the quality of the obtained solution, we computed the Floquet multipliers of the system (i.e.,

3. The generic manifold  $\Sigma \in \mathbb{R}^n$  is a set of points in  $\mathbb{R}^n$  that satisfy a system of  $m$  scalar equations, e.g.,  $\sigma(\cdot) = 0$ , where  $\sigma(\cdot) : \mathbb{R}^m \rightarrow \mathbb{R}^n$  for some  $m \leq n$  [28]. In our example,  $m = 1$ .

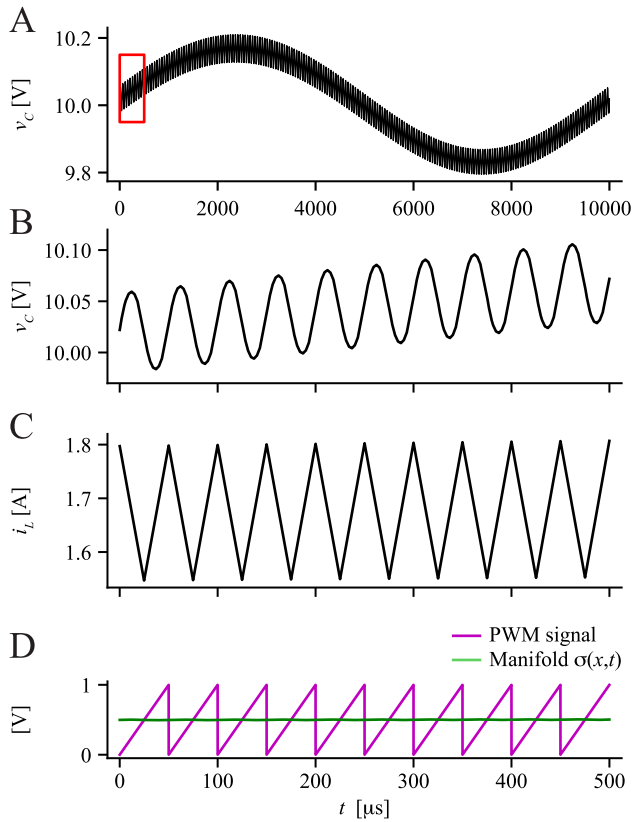


**FIGURE 5.** Dynamics of the PWM buck converter with PI controller. (A) Capacitor voltage  $v_C(t)$  over one long period  $T_S = 1/f_S = 10$  ms. (B-D) Zoom of the system dynamics in the first  $500 \mu\text{s}$  (boxed region in A): capacitor voltage  $v_C(t)$  (B), inductor current  $i_L(t)$  (C), and PWM sawtooth reference signal (magenta) and  $\sigma(x, t)$  manifold (green) determining the switching instants of the system (D). In this example, the PWM period was set to  $T_f = 50 \mu\text{s}$ .

the eigenvalues of the fundamental matrix at the end of the integration period) and the root mean squared error (RMSE) over the envelope points. The latter is defined as

$$\text{RMSE} = \sqrt{\frac{1}{N_{\text{env}}} \sum_{k=1}^{N_{\text{env}}} (x(\hat{t}_k) - \hat{x}(\hat{t}_k))^2}, \quad (15)$$

where  $x$  and  $\hat{x}$  are the conventional and envelope solutions, respectively, and  $\{\hat{t}_k\}$  is the set of  $N_{\text{env}}$  points over which the envelope solution is computed (for this example  $N_{\text{env}}$  ranged from 13 to 26, depending on the ratio between frequencies). We found a good agreement between the conventional and envelope-accelerated cases, as shown in Table 1. Additionally, it is worth noticing that the speed-up of the time to solution shown in Fig. 6A is irrespective of the fact that for some combinations of the parameters the number of iterations required to satisfy the tolerance constraints is greater in the envelope-based method than in the conventional one, as can be seen in Table 1.

### C. ASK/OOK RF MODULATOR

As another example to test the applicability and performance of our method, we consider the ASK/OOK wireless transmitter shown in Fig. 7 and described in detail in [37]–[39]. The

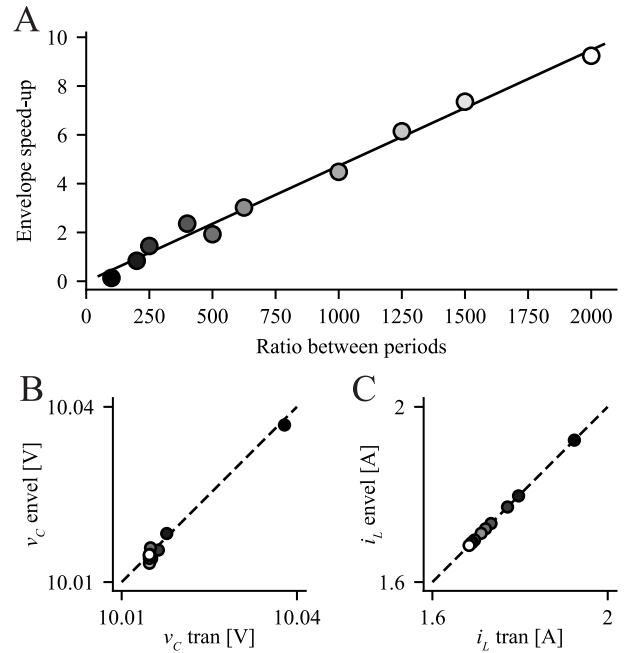


**FIGURE 6.** (A) Speed-up of the time to solution as a function of the ratio between slow and fast oscillation periods. (B, C) Initial condition of the stable limit cycle obtained as a solution of the shooting analysis, for the  $v_C$  and  $i_L$  state variables, for the conventional ( $x$ -axis) and envelope-accelerated ( $y$ -axis) algorithms. Dots represent individual ratios between fast and slow periods and are color-coded as in (A). The dashed line is the identity line and is used to highlight the excellent agreement between the solutions found using the two different algorithms.

**TABLE 1.** Summary of the agreement between conventional and envelope-accelerated shooting analysis for the buck converter shown in Fig. 4, as a function of the ratio between fast and slow oscillation periods. “ $\mu$  tran” and “ $\mu$  envel” are the largest Floquet multiplier of the stable limit cycle obtained without and with envelope-based acceleration, respectively. The rightmost column contains the number of iterations required by the conventional and envelope-accelerated algorithms, respectively, to reach convergence with a tolerance  $< 10^{-3}$ .

Ratio	$\mu$ tran	$\mu$ envel	RMSE $v_C$	RMSE $i_L$	Iterations
100	0.5170	0.5170	$1.14 \times 10^{-3}$	$1.61 \times 10^{-4}$	3, 13
200	0.5135	0.5131	$1.01 \times 10^{-3}$	$1.93 \times 10^{-4}$	3, 4
250	0.5131	0.5136	$1.04 \times 10^{-3}$	$1.89 \times 10^{-4}$	3, 3
400	0.5126	0.5117	$1.48 \times 10^{-3}$	$3.09 \times 10^{-4}$	3, 3
500	0.5125	0.5124	$1.42 \times 10^{-3}$	$3.12 \times 10^{-4}$	3, 4
625	0.5125	0.5128	$9.82 \times 10^{-4}$	$2.15 \times 10^{-4}$	3, 3
1000	0.5124	0.5167	$1.83 \times 10^{-3}$	$3.29 \times 10^{-4}$	3, 3
1250	0.5124	0.5116	$1.86 \times 10^{-4}$	$3.04 \times 10^{-5}$	3, 3
1500	0.5124	0.5127	$5.07 \times 10^{-4}$	$1.14 \times 10^{-4}$	3, 3
2000	0.5124	0.5076	$5.85 \times 10^{-4}$	$1.00 \times 10^{-4}$	3, 3

circuit is modeled by  $N = 8$  ODEs and, as in [39], the drain-source current  $i_{DS}$  of the MOSFETs and the current  $i_D$  of the diode are given by the following simplified nonlinear models:

$$i_{DS}(v_{GS}, v_{DS}) = \frac{\beta}{2} [v + \ln(e^v + e^{-v})] \tanh(\alpha v_{DS})$$

$$i_D(v_D) = I_S \left( e^{\frac{v_D}{nV_{Temp}}} - 1 \right),$$

where  $v_{GS}$  and  $v_{DS}$  are the MOSFETs gate-source and drain-source voltages, respectively,  $v = K_T(v_{GS} - V_T)$  and  $v_D$  is the diode voltage. The parameters of the circuit are given in the caption of Fig. 7.



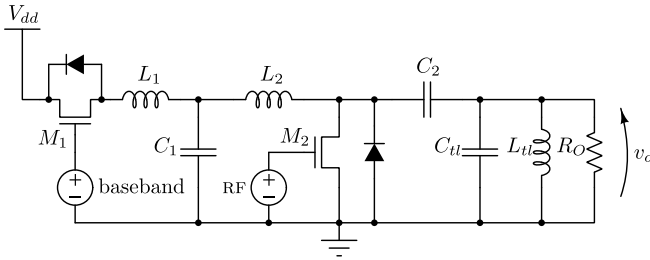


**FIGURE 7.** The schematic of the ASK/OOK RF modulator. Fixed parameter values are:  $V_{dd} = 1.8$  V,  $L_1 = 20$  nH,  $L_2 = 20$  nH,  $C_1 = 500$  pF,  $C_2 = 1$  nF,  $C_{pl} = 1$  fF,  $L_{pl} = (2\pi f_f)^{-2}/C_{pl}$ ,  $R_O = 300$   $\Omega$ ,  $f_s = 1$  MHz,  $f_f = 2$  GHz,  $\alpha = 1$  V $^{-1}$ ,  $\beta = 25$  mA,  $K_T = 2$  V $^{-1}$ ,  $V_T = 1$  V,  $I_S = 1$   $\mu$ A,  $\eta = 2$ ,  $V_{Temp} = 26$  mV.

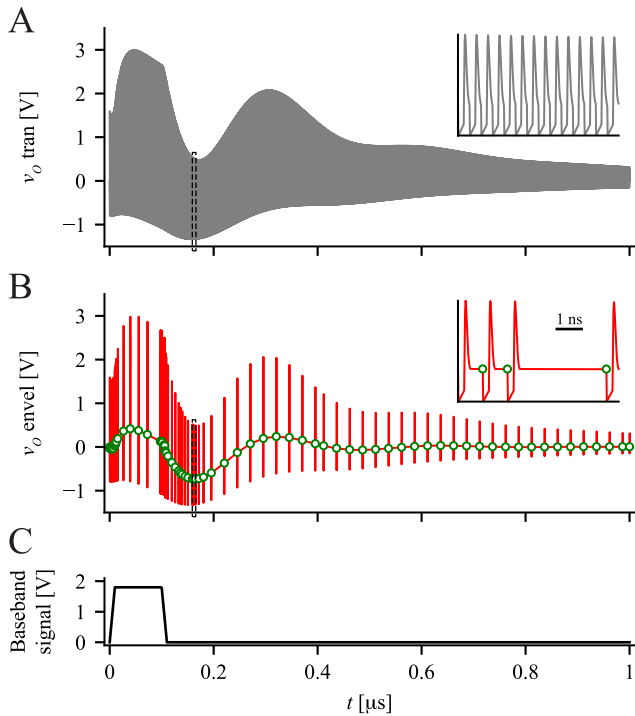


**FIGURE 8.** Example dynamics of the ASK/OOK RF modulator. (A) Output voltage  $v_o$  of the modulator obtained with conventional integration techniques. (B) Envelope of the output voltage  $v_o$  (green markers) and single period integrations starting from the envelope points (red trace). Insets in (A) and (B) are zooms of the black dashed regions. (C) Baseband signal with 10% duty-cycle.

In our implementation we set the frequency of the RF carrier  $f_f = 2$  GHz and we modeled the baseband digital data source as a square wave characterized by a frequency  $f_s = 1$  MHz and a duty cycle of 0.1 (Fig. 8C). An example of the dynamics of the modulator is shown in Fig. 8, obtained with conventional integration of the system (Fig. 8A), and by application of the EFM (Fig. 8B, where the LTE of the variational system was not computed since it does not display periodic oscillatory behavior). Notice that in the latter only the green circular markers constitute the envelope solution. The red trace was obtained *a posteriori* by conventional integration of the system using as initial conditions the EFM points. In the specific case presented in Fig. 8, the speed-up attributable to the usage of the EFM with respect to the conventional SH method was approximately  $4.5 \times$ . The proposed

**TABLE 2.** Comparison of the Floquet multipliers of the ASK/OOK RF modulator obtained at the final iteration of the conventional (“tran” column) and envelope-accelerated (“envel” column) shooting analysis.

Multiplier	tran	envel
1	$2.187 \times 10^{-2}$	$2.266 \times 10^{-2}$
2	$1.194 \times 10^{-3}$	$1.165 \times 10^{-3}$
3	$6.889 \times 10^{-6}$	$7.722 \times 10^{-6}$

**TABLE 3.** RMSE of the state variables of the ASK/OOK RF modulator computed over  $N_{env} = 89$  points. The currents are those flowing in the inductors, whereas the voltages are node potentials in the Modified Nodal Analysis.  $v_{CM_1}$  and  $v_{CM_2}$  are the voltages across the parasitic capacitors present in the model of MOSFETS  $M_1$  and  $M_2$ .

$i_{L_{pl}}$	$i_{L_1}$	$i_{L_2}$	$v_o$
$1.30 \times 10^{-3}$	$2.85 \times 10^{-4}$	$1.26 \times 10^{-3}$	$1.00 \times 10^{-1}$
$v_{C_1}$	$v_{C_2} + v_o$	$V_{DD} - v_{CM_1}$	$v_{CM_2}$
$6.45 \times 10^{-2}$	$6.12 \times 10^{-2}$	$6.77 \times 10^{-2}$	$6.11 \times 10^{-2}$

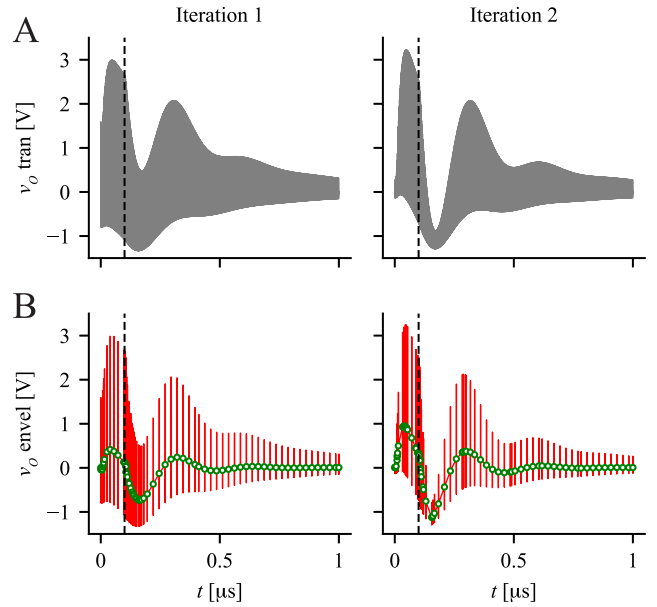


**FIGURE 9.** Shooting analysis of the ASK/OOK RF modulator. (A) Output voltage  $v_o$  obtained with the conventional shooting algorithm over the two iterations it took the algorithm to converge to the steady-state solution of the circuit. (B) Same as A, but for envelope-based shooting. As in Fig. 8, the envelope solution is composed only of the green markers, whereas the red trace is a concatenation of single period solutions obtained *a posteriori* by means of conventional integration starting from the envelope solution points. In all panels, the vertical dashed line indicates the instant in which the baseband signal switches from the value  $V_{dd}$  to 0.

method converged to a stable periodic solution in two iterations. In Fig. 9 the top panels contain simulation results obtained with the conventional shooting algorithm, while the bottom ones show the corresponding integrations performed by means of the EFM.

We see a good qualitative and quantitative agreement with the solution obtained by conventional means. As a further check of the quality of the results obtained by means of the envelope-accelerated shooting analysis, we computed the Floquet multipliers of the steady-state limit cycle obtained at the end of the shooting procedure: those greater than  $10^{-6}$  are reported in Table 2. We also measured the RMSE between conventional and envelope-accelerated solutions on the envelope points, as summarized in Table 3. Taken together, these

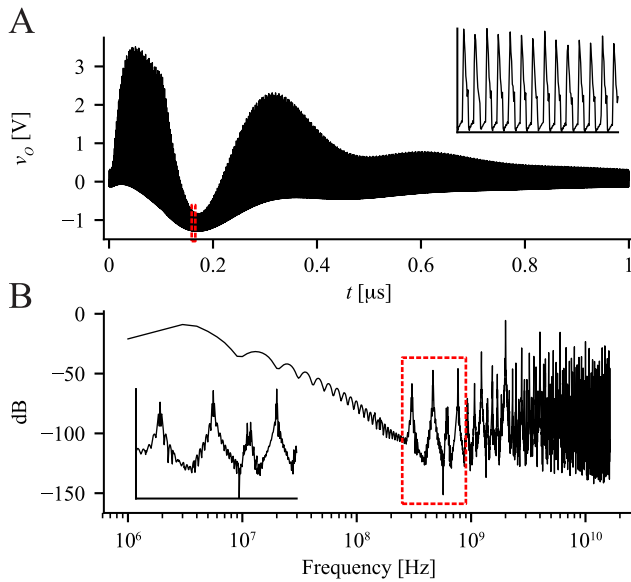


**FIGURE 10.** Harmonic balance analysis of the ASK/OOK RF modulator. (A) Output voltage  $v_o$  obtained with the HB method. Inset, enlargement of the solution in the boxed region of panel A; notice the low accuracy of the solution due to the reduced number of harmonics employed in the HB analysis. (B) Frequency spectrum of the output voltage  $v_o$  shown in A. Inset, enlargement of the boxed region shown in B.

measures highlight the good agreement between the solutions obtained with the two approaches.

Finally, to quantify the efficiency of the proposed method, we used HB on the same circuit and compared simulation times. Given the ratio of  $2\text{GHz}/1\text{MHz} = 2000$  between the two input signals, we decided to employ 16 harmonics to represent the spectrum of the input signal at  $f_i$ : due to the fast rising and falling fronts of the input signal, however, this represents a relatively low figure, and will be reflected in the accuracy of the computed solution. Due to the frequency ratio we thus used a total of 32224 harmonics, leading to an HB problem composed of 491505 unknowns, which requires a highly efficient and specialised solver [40]. Note that this number of harmonics is the minimum one that leads to a solution with an acceptable accuracy. A fair comparison with SH would require more harmonics.

The HB solution is shown in Fig. 10A and can be compared with that obtained by the proposed shooting-envelope algorithm. The CPU time spent was more than 30 times that of the proposed method. We see that, due to the limited number of harmonics, the HB solution is less accurate, as can be seen clearly from the inset of Fig. 10A.

One might object that we could have used a multi-tone harmonic balance method: however, the spectrum of the output voltage  $v_o$  shown in Fig. 10B is not “band-well-separated”, but rather displays a significant magnitude over a wide range of frequencies. This in turn would substantially reduce the potential gain offered by a multi-tone method.

## V. CONCLUSION

In this paper, we have shown how to extend the SH method by means of the EFM to compute the steady-state limit-cycle

solution of nonlinear systems characterized by the presence of two very different time scales. As examples of the applicability of our method, we considered the class of electrical circuits referred to as slow-fast, which exhibit a fast periodic behaviour enveloped by a slowly varying waveform. Typical circuits falling into this class—such as PLLs and SMPS—are driven by two or more signals at very different frequencies, which make the computation of the steady-state solution by means of conventional time-domain simulations very time consuming, even when the SH method, without envelope-following-based acceleration, is employed.

The key point of our algorithm is the replacement of the conventional time-domain simulation performed in each iteration of the SH method with a more efficient EFM analysis. We have shown that the speed-up that can be achieved is approximately one order of magnitude, already in circuits composed by a relatively low number of components. We expect the gain to be substantially larger when real-world circuits are employed.

The proposed algorithm can easily be employed in several fields of application, such as hybrid power systems, where the electrical quantities are simultaneously integrated in the slow dq-frame and in the fast three-phase frame [41].

## APPENDIX SEMI-EXPLICIT INDEX-1 DAE AND ODE

To describe the dynamical behaviour of a generic well-posed smooth non-autonomous analog circuit, the following semi-explicit index-1 DAE can be derived

$$\begin{cases} \dot{x} = f(x, y, t) \\ q(x, y, t) = 0 \\ x(t_0) = x_0 \\ q(x_0, y_0, t_0) = 0, \end{cases} \quad (16)$$

where  $x(t) \in \mathbb{R}^n$  are the circuit *differential* state variables,  $y(t) \in \mathbb{R}^m$  are the *algebraic* variables,  $f: \mathbb{R}^{n+m+1} \rightarrow \mathbb{R}^n$ , and  $q: \mathbb{R}^{n+m+1} \rightarrow \mathbb{R}^m$ . In the case of smooth circuits,  $f$  and  $q$  are assumed to be continuously differentiable in their definition domain and their partial derivatives matrices are referred to as  $f_x, f_y, f_t, q_x, q_y$ , and  $q_t$ . As an example,  $f_{x_{jk}} = \partial f_j / \partial x_k$ , for  $j, k = 1, \dots, n$ . According to the implicit function theorem, if  $q(x^*, y^*, t^*) = 0$ , provided that  $q_y(x^*, y^*, t^*)$  is not singular, a unique and smooth function  $\gamma: \mathbb{R}^{n+1} \rightarrow \mathbb{R}^m$  exists so that  $y^* = \gamma(x^*, t^*)$ . If so, it is possible to rewrite Eq. (16) as

$$\begin{cases} \dot{x} = f(x, \gamma(x, t), t) \equiv F(x, t) \\ x(t_0) = x_0. \end{cases} \quad (17)$$

Some considerations can be made also concerning the computation of the sensitivity of the generic solution of Eq. (16) w.r.t. a system parameter. Assume that  $(x_s(t), y_s(t))$  is the solution of Eq. (16) for  $t \in [t_0, t_1]$ . The sensitivity of the solution with respect to  $p \in \mathbb{R}$  can be

computed by exploiting Eq. (16) as

$$\begin{cases} \frac{d}{dp} \dot{x}|_{x=x_s} = f_x|_{x=x_s} \frac{dx}{dp} + f_y|_{y=y_s} \frac{dy}{dp} \\ q_x|_{x=x_s} \frac{dx}{dp} + q_y|_{y=y_s} \frac{dy}{dp} = 0 \\ \frac{dx_0}{dp} = u_0. \end{cases} \quad (18)$$

By introducing new variables  $u = dx/dp$  and  $w = dy/dp$  and interchanging the derivative order, we obtain

$$\begin{cases} \dot{u} = f_x|_{x=x_s} u + f_y|_{y=y_s} w \\ q_x|_{x=x_s} u + q_y|_{y=y_s} w = 0 \\ u(t_0) = u_0. \end{cases} \quad (19)$$

Equation (19) represents a *new* DAE whose solution is the sensitivity of the solution with respect to the  $p$  parameter given the  $u_0$  initial condition. Note that Eq. (19) is *linear* and time-varying. Since we assumed that  $q_y$  is non-singular, we achieve

$$w = -q_y^{-1} q_x u. \quad (20)$$

The substitution of Eq. (20) in Eq. (19) yields

$$\begin{cases} \dot{u} = \left( f_x|_{x=x_s} - f_y|_{x=x_s} q_y^{-1}|_{x=x_s} q_x|_{x=x_s} \right) u \\ u(t_0) = u_0. \end{cases} \quad (21)$$

The  $u(t)$  solution of the linear time-varying differential equation Eq. (21) leads to the sensitivity of  $x_s(t)$  with respect to the  $p$  parameter; the  $w(t)$  sensitivity of  $y_s(t)$  can be subsequently derived from Eq. (20). If one is interested in evaluating the sensitivity of the solution with respect to the initial conditions, and this is the case of the SH method introduced in Section Eq. II-A, it is sufficient to introduce the matrices  $\Phi(t, t_0) \in \mathbb{R}^{n \times n}$  and  $\Psi(t, t_0) \in \mathbb{R}^{m \times n}$  and solve

$$\begin{cases} \dot{\Phi}(t, t_0) = \left( f_x|_{x=x_s} - f_y|_{x=x_s} q_y^{-1}|_{x=x_s} q_x|_{x=x_s} \right) \Phi(t, t_0) \\ \Phi(t_0, t_0) = \mathbb{1}, \end{cases} \quad (22)$$

where  $\mathbb{1}$  is the  $n \times n$  identity matrix. The sensitivity matrix of  $y$  with respect to  $x_0$  is given by  $\Psi(t, t_0) = -q_y^{-1}|_{x=x_s} q_x|_{x=x_s} \Phi(t, t_0)$ .

## REFERENCES

- [1] A. L. Lacaita, S. Levantino, and C. Samori, *Integrated Frequency Synthesizers for Wireless Systems*. New York, NY, USA: Cambridge Univ. Press, 2007.
- [2] J. F. Oliveira, "Radio frequency and microwave numerical simulation techniques based on multivariate formulations," *Appl. Math. Comput.*, vol. 294, pp. 238–252, Feb. 2017.
- [3] K. Kundert, J. White, and A. Sangiovanni-Vincentelli, *Steady-State Methods for Simulating Analog and Microwave Circuits*. New York, NY, USA: Kluwer Acade. Publ., 1990.
- [4] Y. Saad and H. Schultz, "Gmres: A generalized minimal residual algorithm for solving non symmetric linear systems," *SIAM J. Sci. Stat. Comput.*, vol. 7, pp. 856–869, Jul. 1986.
- [5] F. Bizzarri, A. Brambilla, and G. S. Gajani, "Steady state computation and noise analysis of analog mixed signal circuits," *IEEE Trans. Circuits Syst. I, Reg. Papers*, vol. 59, no. 3, pp. 541–554, Mar. 2012.
- [6] F. Bizzarri, A. Brambilla, and G. S. Gajani, "Extension of the variational equation to analog/digital circuits: Numerical and experimental validation," *Int. J. Circuit Theory Appl.*, vol. 41, no. 7, pp. 743–752, 2013.
- [7] F. Bizzarri, A. Brambilla, and L. Codecasa, "Shooting by a two-step Galerkin method," *IEEE Trans. Circuits Syst. I, Reg. Papers*, vol. 66, no. 1, pp. 383–390, Jan. 2019.
- [8] D. D. Morrison, J. D. Riley, and J. F. Zancanaro, "Multiple shooting method for two-point boundary value problems," *Commun. ACM*, vol. 5, pp. 613–614, Dec. 1962.
- [9] H. G. Brachtendorf, G. Welsch, R. Laur, and A. Bunse-Gerstner, "Numerical steady state analysis of electronic circuits driven by multiple signals," *Elect. Eng.*, vol. 79, pp. 103–112, Apr. 1996.
- [10] J. Roychowdhury, "Analyzing circuits with widely separated time scales using numerical PDE methods," *IEEE Trans. Circuits Syst. I*, vol. 48, no. 5, pp. 578–594, May 2001.
- [11] T. Mei, J. Roychowdhury, T. S. Coffey, S. A. Hutchinson, and D. M. Day, "Robust, stable time-domain methods for solving MPDEs of fast/slow systems," *IEEE Trans. Comput.-Aided Design Integr. Circuits Syst.*, vol. 24, no. 2, pp. 226–239, Feb. 2005.
- [12] M. A. Farhan, M. S. Nakhla, E. Gad, and R. Achar, "Parallel high-order envelope-following method for fast transient analysis of highly oscillatory circuits," *IEEE Trans. Very Large Scale Integr. (VLSI) Syst.*, vol. 25, no. 11, pp. 261–270, Jan. 2017.
- [13] T. Mei and J. Roychowdhury, "A time-domain oscillator envelope tracking algorithm employing dual phase conditions," *IEEE Trans. Comput.-Aided Design Integr. Circuits Syst.*, vol. 27, no. 1, pp. 59–69, Jan. 2008.
- [14] P. Feldmann and J. Roychowdhury, "Computation of circuit waveform envelopes using an efficient, matrix-decomposed harmonic balance algorithm," in *Proc. Int. Conf. Comput.-Aided Design*, Nov. 1996, pp. 295–300.
- [15] J. C. Pedro and N. B. Carvalho, "Simulation of RF circuits driven by modulated signals without bandwidth constraints," in *IEEE MTT-S Int. Microw. Symp. Dig. Tech.*, vol. 3, Jun. 2002, pp. 2173–2176.
- [16] E. Ngoya and R. Larcheveque, "Envelope transient analysis: A new method for the transient and steady state analysis of microwave communication circuits and systems," in *IEEE MTT-S Int. Microw. Symp. Dig. Tech.*, vol. 3, Jun. 1996, pp. 1365–1368.
- [17] W. Dong and P. Li, "A parallel harmonic-balance approach to steady-state and envelope-following simulation of driven and autonomous circuits," *IEEE Trans. Comput.-Aided Design Integr. Circuits Syst.*, vol. 28, no. 4, pp. 490–501, Apr. 2009.
- [18] S. Sancho, A. Suarez, and J. Chuan, "General envelope-transient formulation of phase-locked loops using three time scales," *IEEE Trans. Microw. Theory Techn.*, vol. 52, no. 4, pp. 1310–1320, Apr. 2004.
- [19] J. F. Oliveira and J. C. Pedro, "A multiple-line double multirate shooting technique for the simulation of heterogeneous rf circuits," *IEEE Trans. Microw. Theory Techn.*, vol. 57, no. 2, pp. 421–429, Feb. 2009.
- [20] J. F. Oliveira and J. C. Pedro, "Efficient RF circuit simulation using an innovative mixed time-frequency method," *IEEE Trans. Microw. Theory Techn.*, vol. 59, no. 4, pp. 827–836, Apr. 2011.
- [21] M. A. Farhan, E. Gad, M. S. Nakhla, and R. Achar, "High order and a-stable envelope following method for transient simulations of oscillator circuits," *IEEE Trans. Microw. Theory Techn.*, vol. 62, no. 12, pp. 3309–3317, Dec. 2014.
- [22] L. R. Petzold, "An efficient numerical method for highly oscillatory ordinary differential equations," *SIAM J. Numer. Anal.*, vol. 18, no. 3, pp. 455–479, 1981.
- [23] A. Brambilla and P. Maffezzoni, "Envelope-following method to compute steady-state solutions of electrical circuits," *IEEE Trans. Circuits Syst. I, Fundam. Theory Appl.*, vol. 50, no. 3, pp. 407–417, Mar. 2003.
- [24] K. Kundert, J. White, and A. Sangiovanni-Vincentelli, "An envelope-following method for the efficient transient simulation of switching power and filter circuits," in *Proc. IEEE Int. Conf. Comput.-Aided Design (ICCAD-89) Dig. Tech. Papers*, Nov. 1988, pp. 446–449.
- [25] J. Vlach and K. Singhal, *Computer Methods for Circuit Analysis and Design*. New York, NY, USA: Van Nostrand Reinhold Company, 1983.
- [26] U. Parlitz and W. Lauterborn, "Period-doubling cascades and devil's staircases of the driven van der Pol oscillator," *Phys. Rev. A*, vol. 36, no. 3, p. 1428, 1987.
- [27] P. Holmes and D. Rand, "Bifurcations of the forced van der Pol oscillator," *Quart. Appl. Math.*, vol. 35, no. 4, pp. 495–509, 1978.
- [28] Y. A. Kuznetsov, *Elements of Applied Bifurcation Theory*, 3rd ed. New York, NY, USA: Springer-Verlag, 2004.
- [29] E. Jones, T. Oliphant, and P. Peterson, "Scipy: Open source scientific tools for Python," 2001.

- [30] F. Bizzarri, A. Brambilla, and F. Milano, "The probe-insertion technique for the detection of limit cycles in power systems," *IEEE Trans. Circuits Syst. I, Reg. Papers*, vol. 63, no. 2, pp. 312–321, Feb. 2016.
- [31] M. Farkas, *Periodic Motions*. New York, NY, USA: Springer-Verlag, 1994.
- [32] T. J. Aprille and T. N. Trick, "Steady-state analysis of nonlinear circuits with periodic inputs," *Proc. IEEE*, vol. 60, no. 1, pp. 108–114, Jul. 1972.
- [33] T. Aprille and T. Trick, "A computer algorithm to determine the steady-state response of nonlinear oscillators," *IEEE Trans. Circuit Theory*, vol. CT-19, no. 4, pp. 354–360, Jul. 1972.
- [34] M. Di Bernardo, C. Budd, A. Champneys, and P. Kowalczyk, *Piecewise-Smooth Dynamical Systems, Theory and Applications*. Heidelberg, Germany: Springer-Verlag, 2008.
- [35] F. Bizzarri, A. Brambilla, and G. S. Gajani, "Lyapunov exponents computation for hybrid neurons," *J. Comput. Neurosci.*, vol. 35, no. 2, pp. 201–212, 2013.
- [36] A. El Aroudi, M. Debbat, R. Giral, G. Olivar, L. Benadero, and E. Toribio, "Bifurcations in DC-DC switching converters: Review of methods and applications," *Int. J. Bifurcation Chaos*, vol. 15, pp. 1549–1578, Nov. 2011.
- [37] Y.-D. Lee *et al.*, "ASK modulator for RFID system using a novel variable DGS resonator," in *Proc. IEEE Eur. Radar Conf.*, 2007, pp. 381–384.
- [38] J. Ryu, M. Kim, J. Lee, B.-S. Kim, M.-Q. Lee, and S. Nam, "Low power OOK transmitter for wireless capsule endoscope," in *Proc. IEEE/MTT-S Int. Microw. Symp.*, 2007, pp. 855–858.
- [39] D. Ferreira, J. F. Oliveira, and J. C. Pedro, "A novel time-domain CAD technique based on automatic time-slot division for the numerical simulation of highly nonlinear RF circuits," *IEEE Trans. Microw. Theory Techn.*, vol. 62, no. 1, pp. 18–27, Jan. 2014.
- [40] F. Bizzarri and A. Brambilla, "PAN and MPanSuite: Simulation vehicles towards the analysis and design of heterogeneous mixed electrical systems," in *Proc. IEEE New Gener. CAS (NGCAS)*, 2017, pp. 1–4.
- [41] F. Bizzarri and A. Brambilla, "Generalized power flow analysis of electrical power systems modeled as mixed single-phase/three-phase sub-systems," *IEEE Trans. Power Syst.*, vol. 35, no. 2, pp. 1284–1293, Mar. 2020.



**DANIELE LINARO** received the M.Sc. degree in electronic engineering and the Ph.D. degree in electrical engineering from the University of Genoa, Italy, in 2007 and 2011, respectively. Since 2018, he has been an Assistant Professor with the Department of Electronics, Information Technology and Bioengineering, Polytechnic of Milan. His main research interests are currently in the area of circuit theory and nonlinear dynamical systems, with applications to electronic oscillators and power systems and computational neuroscience, in particular biophysically realistic single-cell models of neuronal cells.



**DAVIDE DEL GIUDICE** (Graduate Student Member, IEEE) was born in Milan, Italy, in July 1993. He received the B.S. and M.S. degrees (*cum laude*) in electrical engineering from Politecnico di Milano, Italy, in 2015 and 2017, respectively, where he is currently pursuing the Ph.D. degree with the Department of Electronics, Information and Bioengineering. His main research activities are related to simulation techniques specifically tailored to electric power systems characterized by a high penetration of renewable energy sources, such as HVDC systems.



**ANGELO BRAMBILLA** (Member, IEEE) received the Dr.Ing. degree in electronics engineering from the University of Pavia, Pavia, Italy, in 1986. He is a Full Professor with the Dipartimento di Elettronica, Informazione e Bioingegneria, Politecnico di Milano, Milan, Italy, where he has been working in the areas of circuit analysis, simulation, and modeling.



**FEDERICO BIZZARRI** (Senior Member, IEEE) was born in Genoa, Italy, in 1974. He received the Laurea (M.Sc.) five-year degree (*summa cum laude*) in electronic engineering and the Ph.D. degree in electrical engineering from the University of Genoa, Genoa, in 1998 and 2001, respectively. Since October 2018, he has been an Associate Professor with the Electronic and Information Department, Politecnico di Milano, Milan, Italy. He is a Research Fellow with the Advanced Research Center on Electronic Systems for Information and Communication Technologies "E. De Castro," University of Bologna, Italy. He served as an Associate Editor for the IEEE TRANSACTIONS ON CIRCUITS AND SYSTEMS—PART I: REGULAR PAPERS from 2012 to 2015 and he was awarded as one of the 2012–2013 Best Associate Editors of this journal.